Dan Zhang · Qiang Xu · Adam Bezuijen · Guang Zheng · Hongxian Wang

Internal deformation monitoring for centrifuge slope model with embedded FBG arrays

Abstract The fiber Bragg grating (FBG) sensing technology was utilized for internal deformation monitoring in a centrifuge test of soil slope. An array of FBG sensors were encapsulated into a sensing fiber with a diameter of 0.9 mm. A pullout test was designed to investigate the frictional behavior between the sensing fiber and soil. It was concluded that, for a certain value of overburden pressure, the fiber strain is equal to the strain of soil as long as the fiber strain is less than its peak value in the pullout test. The sensing fibers were embedded directly into a slope centrifuge model to monitor the internal strain distribution and its variation. It can be found that the horizontal sensors were stretched extremely and the vertical sensors were compressed distinctly near a potential slip surface. Thus, it is possible to evaluate the soil internal deformation as well as the failure of the slope model by using FBG sensing technology. This is verified by a comparison between the results of FBGs and that of a numerical simulation. According to these preliminary results, discussions and recommendations for further research are presented.

Introduction

Centrifuge testing is a geotechnical modeling method that plays a crucial role in investigating the behavior of soil and structures because it can reproduce the prototype stress field and the deformation process. It has been used in studying slope instability (Ling et al. 2009). In centrifuge tests, as in full-scale geotechnical systems, different transducers are employed to monitor, for example, displacements, pore pressures, contact stresses, and structural resultants, during the flight of the centrifuge model (Muir Wood 2004). Linear variable differential transformers (LVDTs), noncontact laser techniques, close-range photogrammetry, and particle image velocimetry (PIV) are the common methods for high-precision displacement recording (White and Bolton 2002). These methods are mainly used for displacement measurements on the external surface of models. In fact, the external displacements of models are the result of internal deformation. Measurements of the distribution of internal deformation and its variation can be helpful for comprehensive model analysis. Typically, if the model is designed according to the plane strain assumption, a transparent Perspex wall with grid marks is built into one side of the model for measuring the internal soil deformation (Take et al. 2004). Thereafter, an image analysis technique, such as PIV, is adopted for analysis of soil deformation in the model. In some cases, the model is constructed to include elements such as layers of colored sand, dry spaghetti, or similar objects so that internal deformation can be examined by cutting the model after the test is completed (Zornberg et al. 1997) or by applying an x-ray CT-scan (Kruse and Bezuijen 1998). If the internal deformation of a centrifuge model is three-dimensional, a Perspex wall will not reveal most of the deformation. Even the use of colored sand or similar indicators does not make it easy to simultaneously record and display the internal deformation process.

Numerous centrifuge tests use in-flight installation of structures to investigate induced effects, excavation-related soil deformation, and interaction with other structures (Sommers and Viswanadham 2009; Ng et al. 2013a, b; Elshafie et al. 2013). Traditional observation methods such as LVDTs and strain gauges can monitor internal deformation, but they produce size effects and so often they are unsuitable for installation within centrifuge models. Along certain directions, and for certain desired positions, measurements of the distribution of the internal deformation can be difficult. Therefore, identifying a new method to monitor the distributions of internal deformations in centrifuge models and variation for different conditions, especially relatively small values at early stages, would constitute a substantial advancement. Such monitoring can describe the development of failures, the mechanisms involved, and the main factors that influence the behavior of the model.

Triggering factors for landslides include rainfall, groundwater, geometry changes, seismic loading, and surcharge (Ortigao and Sayao 2004). When a slope is close to its critical state, any factor can cause the failure of that slope. Centrifuge modeling is utilized to conduct parametric studies to investigate the stability of the model. Based on the reconstructed distribution of in situ stress, deformation, and their variation during testing, it would be helpful to reveal where the internal deformation starts, and how the deformation changes under different conditions. The possible failure mechanisms, types, and processes of the model can also be revealed. In recent years, the adoption of these centrifuge techniques for pre-failure deformation research increased.

In addition, to minimize the size effect of transducers on the centrifuge modeling, the smallest possible transducers must be utilized.

Fiber optic sensing is an innovative and rapidly developing technology that has been successfully applied to performance monitoring in many fields such as civil engineering (Ansari 2007; Lu et al. 2012), geohazards (Wang et al. 2009; Yin et al. 2010; Shi et al. 2011; Habel et al. 2014; Sun et al. 2014), and energy industries (Arsenault et al. 2013; Niewczas and McDonald 2007). Fiber optic sensors have some unique advantages over conventional sensors, including immunity to external electromagnetic (EM) perturbations, high precision, strong durability, and long service lives for long-term monitoring (Bao and Chen 2012). This paper describes a new data collection system that incorporates fiber Bragg grating (FBG)-based fiber optic sensing technology to monitor the internal deformation of a centrifuge testing model. The major components of the system are the FBG interrogator, FBG arrays (FBG sensing fibers), communication fiber, and

wireless signal transmission equipment. A simple centrifuge slope model was constructed to evaluate the performance of the system. The g-level was increased from 1 to 10 g to change the internal deformation of the slope model. The in-flight strains of the FBG sensors were obtained and analyzed. From the strain distributions and their variation, the potential slip surface was deduced and compared with the results of a numerical analysis. Experimental results confirmed that FBG-based fiber optic sensing technology can acquire pre-failure deformation information inside a centrifuge slope model.

Principles of FBG sensing technology

A fiber Bragg grating sensor is fabricated in the core region of a single mode optical fiber (Hill et al. 1978, 1993). As shown in Fig. 1, the refractive index will typically alternate over a defined length. The reflected wavelength λ_B, called the Bragg wavelength, is defined by the following equation:

$$\lambda_B = 2n_e\Lambda \tag{1}$$

where n_e is the effective refractive index of the grating in the fiber core and Λ is the grating period. The Bragg grating acts as a wavelength-selective mirror. When a broadband input signal is injected into the fiber and interacts with the grating, only the wavelength of λ_B can be back-reflected without any perturbations in the other wavelengths.

An FBG is sensitive to axial elongation and temperature, as shown in Equation (2):

$$\frac{\Delta\lambda_B}{\lambda_B} = (1-p_e)\varepsilon + (\alpha_\Lambda-\alpha_n)\Delta T \tag{2}$$

where $\Delta\lambda_B$ is the shift of reflected wavelength ($\lambda'_B - \lambda_B$), p_e is the photoelastic coefficient, α_Λ is the thermal expansion coefficient, and α_n is the thermal modulation of the core refractive index. The shift of reflected wavelength has an accurate linear relationship with the axial strain ε and the change of temperature ΔT.

A number of gratings with different Bragg wavelengths can be inscribed on the same fiber and interrogated by one interrogator, which is called multiplexing (Rao et al. 1995). A multiplexed fiber constitutes a sensor array with different grating periods, Λ_i, $i = 1,2,\ldots,k$, as shown in Fig. 2. The reflected signal contains a series of peaks, each associated with a different Bragg wavelength. Multiplexing is the most critical advantage of FBG because it enables quasi-distributed measurement.

Frictional behavior between the sensing fiber and the soil

Typically, a single mode fiber includes four layers: the core, cladding, buffer, and jacket. The core is a cylindrical silicon thread with a diameter of 8–10 μm, and is surrounded by a transparent cladding material with a lower index of refraction. The buffer is a layer of material used to protect the optical fiber from physical damage and prevent the optical fiber from scattering losses caused by microbends. Before the grating, the buffer is stripped at certain locations specified by the design. The length of the grating zone is 10 mm. To avoid damage to the grating, the grating zone is coated again using some buffer material. For extra protection, an additional layer called the jacket is deployed outside the buffer layer to increase the mechanical strength of the sensing fiber.

In the centrifuge model, the sensors used were a type of FBG array encapsulated into a sensing cable with diameter of 0.9 mm. The sensing fibers were embedded directly into the soil to monitor the internal deformation of the slope model. Accurate representation of the friction behavior between the sensing fiber and the surrounding soil is crucial for measurement quality (Hauswirth et al. 2010). If the deformation of the soil is not totally transferred into the fiber, the relationship between the deformation of soil and that of the sensing fiber must be clarified. To investigate the frictional behavior, a pullout test on the sensing fiber was conducted.

The sensing fiber was embedded in a soil specimen made using the cutting ring, which was 61.8 mm in diameter and 20.0 mm in height. Two holes, each with a diameter of 2 mm,
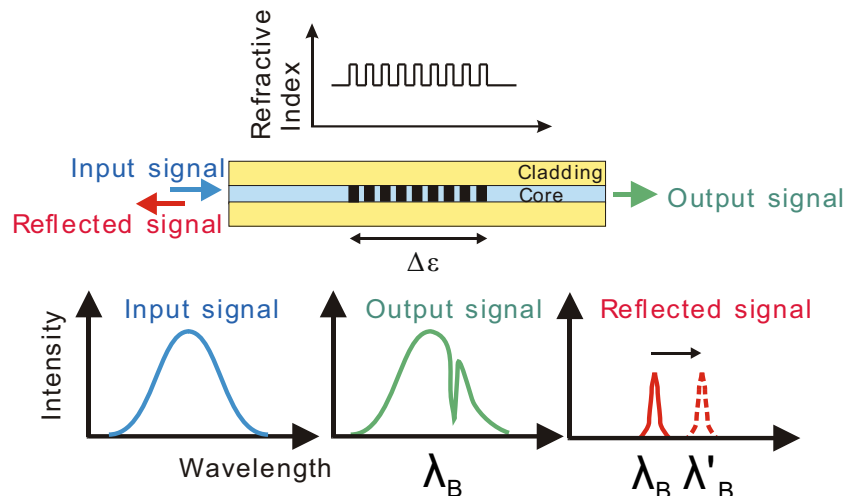

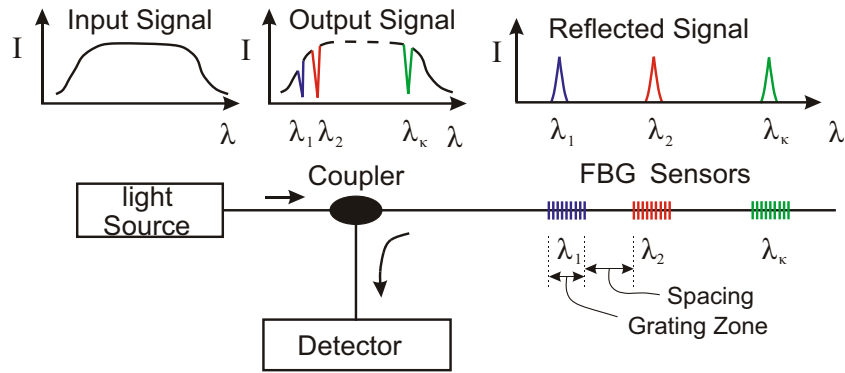**Fig. 1** Fiber Bragg grating

Fig. 2 Multiplexing of FBGs

were drilled into opposite sides of the cutting ring for fiber embedment. The sensing fiber was embedded in the middle of the soil sample by hierarchical compression by using a hydraulic jack. First, half of the required soil was placed into the cutting ring and was compressed to the middle height of the cutting ring. The sensing fiber was then laid straight across the soil surface, and the second layer was compressed using the remaining soil as shown in Fig. 3. The soil was a mixture of 90 % sand and 10 % Kaolin with a dry density of 2.0 g/cm³ and a water content of 10 %. By triaxial shear testing, the cohesion and angle of internal friction were obtained. To obtain the axial stress of the fiber, a Bragg grating was inscribed in the sensing cable. The location of the FBG sensor was just on the edge of cutting ring, as shown in Fig. 3. A pullout force was applied by a step motor on the other side of the fiber; and was measured using a digital force gauge with a measuring range of 50 N and resolution of 0.1 N. During the pullout test, the cutting ring was fixed, and different vertical stresses were applied on the upper surface of the soil sample to simulate the in situ overburden pressure.

Figure 4 presents typical results of a pullout test under a vertical stress of 40 kPa. The peak pullout force is 15 N and the peak FBG strain is approximately 6300 με. The peak of FBG strain lags behind the pullout force peak because the friction between the fiber and soil peaked on the left side first, but after that, the peak

value propagated to the right side as the pullout force increased. It can be deduced from Fig. 5 that FBG strain increases with the vertical stress. The pullout force is the sum of interfacial friction stress on the surface of the sensing fiber embedded in the soil. The interfacial friction stress, static or kinetic, is a function of normal force on the surface of the fiber. When the fiber strain is less than the peak value, it can be assumed that there should not be slippage between the fiber and soil. The fiber's strain should be equal to the strain of soil; if it is not, the deformation of the fiber is not consistent with that of the soil. The ratio between the strain of fiber and the soil indicates the degree to which the deformation is transferred from the soil to the sensing fiber. Therefore, the strain state of the soil can be collected by embedding the fiber into the soil if no large deformation has occurred; this is typical when the strain of the fiber is less than the peak value. Although there is slippage between the fiber and soil, estimation of the deformation as well as of the failure in the model can be calculated from the fiber strain.

Centrifuge slope model test

Model design

This test was undertaken in the geotechnical centrifuge at Chengdu University of Technology, China. The centrifuge has a
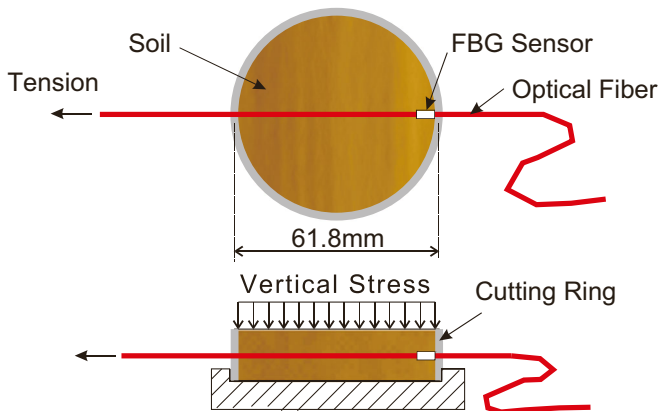

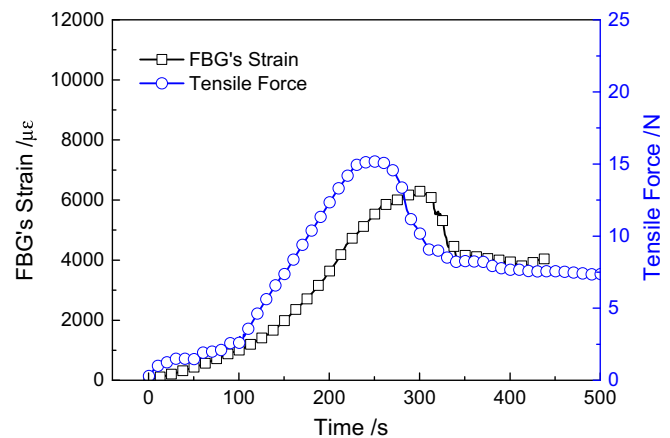**Fig. 3** Layout of fiber pullout test from the soil

Fig. 4 Time–history curve of FBG strain and pullout force under a vertical stress of 40 kPa
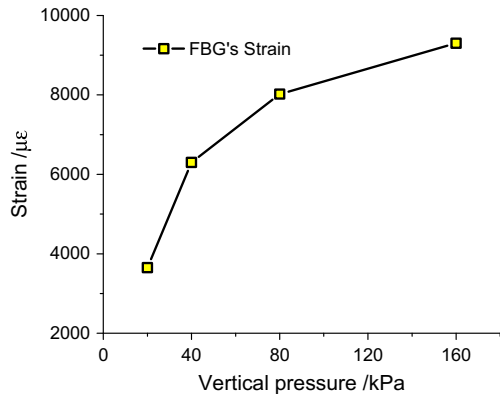
Fig. 5 Relationship between the FBG peak strain and applied vertical stress
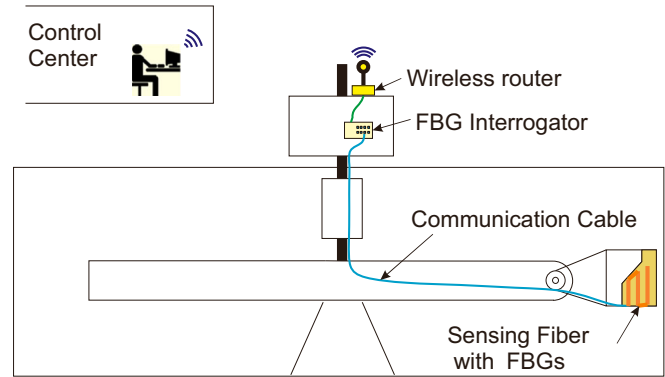

Fig. 7 Configuration of the FBG sensing system for internal deformation monitoring of a centrifuge model

nominal radius of 4.5 m and is capable of accelerating a 2-ton package to 250 g.

A simple centrifuge slope model was designed and developed to verify the possibility of using optical sensing fibers for deformation measurement. The slope model was constructed inside a strong box, with inner dimensions of 100 × 100 × 50 cm (length × height × width). Figure 6 shows the schematic view and the size of the centrifuge slope model. The slope was 1:0.68 (vertical:horizontal) and 38 cm in height. A 22-cm-high soil layer under the slope was included to diminish the influence of the bottom container plate on the deformation of the slope. The soil was a mixture of 90 % fine sand and 10 % Kaolin. Its water content was 10 %. The soil was compacted into the container layer-by-layer with a density of 1.96 g/cm³. The maximum dry density was 1.98 g/cm³, and the minimum dry density was 1.49 g/cm³. The relative density achieved was 66 %.

Seven sensing fibers with 3–5 FBG sensing points on each fiber were embedded into the slope layer-by-layer during the construction of the model. Three displacement transducers, d1, d2, and d3,

were utilized to measure the vertical displacement of the slope surface. After the installation, the sensing fibers outside the model were fixed to the side wall of the container, and the communication fibers were fixed to the centrifuge beam and the center shaft to avoid damage during the flying of the model. The FBG interrogator was installed in the upper instrument cabinet, shown in Fig. 7, to ensure a stable wireless connection with the computer in the control center. Typically, an interrogator should be as close to the central shaft as possible to limit centrifugal force. A wireless router was connected with the FBG interrogator to transmit the wavelengths of FBGs with wireless signals during the test. The configuration of the FBG sensing system is shown in Fig. 7. During the testing, the centrifuge model, fibers, FBG interrogator, and wireless router were all rotating with the centrifuge beam.

FBG sensing fibers

In this study, each sensing fiber used for the measurement of soil strain was a specially designed FBG sensor array of the same type used in the experiment of frictional behavior between the sensing
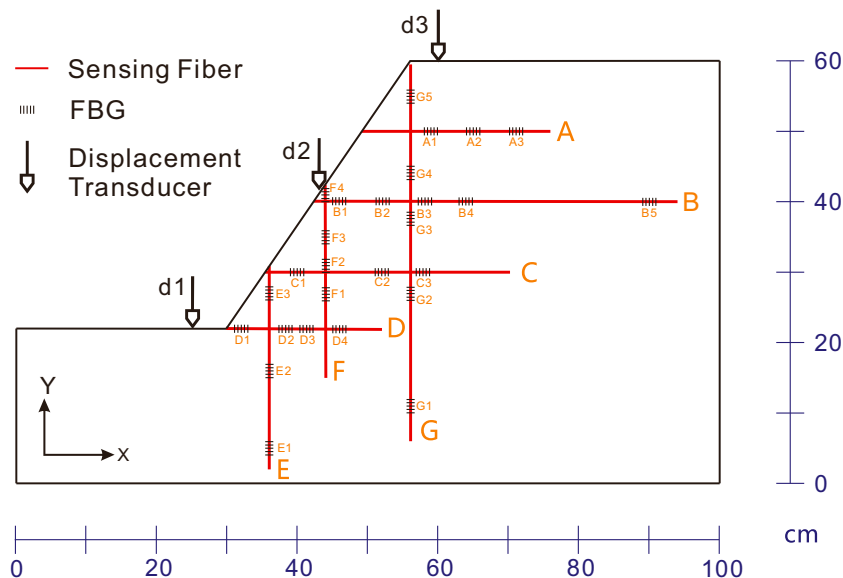

Fig. 6 Schematic view of the centrifuge model (unit: centimeter)

| Grating Zone |

Fig. 8 Encapsulated FBG sensing fiber

fiber and soil. Each sensor array contained four or five gratings (FBGs) with different central wavelengths that were written along a single fiber by using a UV laser. After the gratings had been etched, the FBG sensors were coated with acrylate and encapsulated with Hytrel jackets; the end products were called "FBG sensing fibers." The diameter of each FBG sensing fiber after encapsulation was 0.9 mm and the sensing length of each FBG was 10 mm. The spacing between the FBGs in one fiber was specified for collection of deformation information at certain positions within the model. Figure 8 shows the photo of the encapsulated sensing fiber. The length between the two marked points is the grating zone.

Fiber installation

The slope model was constructed by compacting the soil layer-by-layer. Sensing fibers were embedded in the model horizontally and vertically at the designed locations. Each horizontal sensing fiber was laid straight on the soil surface when the soil was built to the required height. The sensing points were aligned carefully with the designated positions. After placement, each sensing fiber was covered with another layer of soil, and the soil was compacted to the required density. In this model, Fibers A, B, C, and D were installed horizontally. For example, when the height of the model reached 0.22 m (y coordinate), Fiber D was laid on the top surface and the FBG grating points were located at 0.34, 0.39, 0.43, and 0.46 m (x coordinate) according to the design. Similarly, other horizontal fibers were installed at different heights during the construction of the slope.

Regarding the vertical sensing fibers, namely Fibers E, F, and G, a rigid steel rod with a diameter of 1 mm was utilized to install the

Table 1 Position of FBG sensing points in the model

Fibers	Number of FBGs	x coordinate (m)	y coordinate (m)
A	3	0.59, 0.65, 0.71	0.50
B	5	0.46, 0.52, 0.58, 0.64, 0.90	0.40
C	3	0.40, 0.51, 0.62	0.30
D	4	0.34, 0.39, 0.43, 0.46	0.22
E	3	0.36	0.05, 0.16, 0.27
F	4	0.44	0.27, 0.30, 0.35, 0.40
G	5	0.56	0.11, 0.27, 0.38, 0.44, 0.55

sensing fibers vertically during the construction of model. The steel rod was inserted into the soil to a depth of 5 cm and then another 10 cm of the model was constructed. Before the upper layer of soil was filled, one end of the sensing fiber was laid on the surface horizontally and led out of the strong box from the back of the slope. The other end was led upwards along the steel rod with its sensing points at the designated heights. After that, the slope was compacted layer-by-layer. During the construction of the model, the steel rod was pulled out little by little, but its bottom end remained inside the soil. The hole caused by the removal of the rod was filled with the soil compaction. The positions of the FBG sensing points in the model are listed in Table 1. There were 27 FBGs embedded in the slope model.

After the construction of the model, pairs of fibers were spliced to one sensing fiber and connected to the interrogator by optical communication fibers. The central wavelength of each FBG in a single fiber was required to differ as much as possible to prevent spectrum overlapping during the model testing because the interrogator was not able to separate two FBGs with the same central wavelength for wavelength-division multiplexing.

Experimental results and analysis

Strain variations and distributions of FBG sensing fibers

FBG is sensitive to temperature. However, temperature compensation was not undertaken in this note because the temperature was almost constant during the centrifuge tests according to the following reasons. (1) As shown in Figs. 9 and 10, it took no more than 10 min when the g-level was increased from 1 to 10 g. The temperature changes should not be large because the running time of centrifuge is small. (2) The Geotechnical Centrifuge Laboratory at Chengdu University of Technology, China, has a ventilation system to control the temperature. (3) The FBG sensing cables were embedded in the soil, which are not as sensitive as in the air. (4) The temperature sensor in the centrifuge laboratory indicated that the temperature was almost constant during the tests.

Figure 9 shows the strain variations of all horizontal FBGs when the g-level was increased from 1 to 10 g. The FBG sensors were in a tensile state, which indicates that the tensile deformation occurred in the horizontal direction. The maximum strain was measured using sensor B3, approximately 3700 µε, located at (0.58, 0.4), where its overburden pressure was, theoretically, approximately 40 kPa. According to the experimental results in section 3, slippage between the fiber and soil will not occur if the strain is less than 6300 µε. Therefore, it can be deduced that the strain status of the fiber and soil was almost the same, and they deformed simultaneously when the g-level was 10 g. At the same time, the strain values of some FBGs in one fiber were different, which suggests that the soil deformation along the embedded fiber was not the same. Consider Fiber B, which was located at the back of the slope: the strain of sensor B5 at (0.9, 0.4) was relatively small, approximately 300 µε. The strain of B1 at (0.46, 0.4), which was near the surface the slope, was approximately 1500 µε. The strain of other three sensors, B2, B3, and B4, showed a marked rise when the g-level was increased from 1 to 10 g. This suggests that the horizontal deformation of the soil at the locations of B2, B3, and B4 was larger than at other locations. Similar phenomena can also be found for the other sensing fibers. It was estimated that the potential slip surface of this centrifuge slope should have been close to B3 and

(a) Fiber A

(b) Fiber B
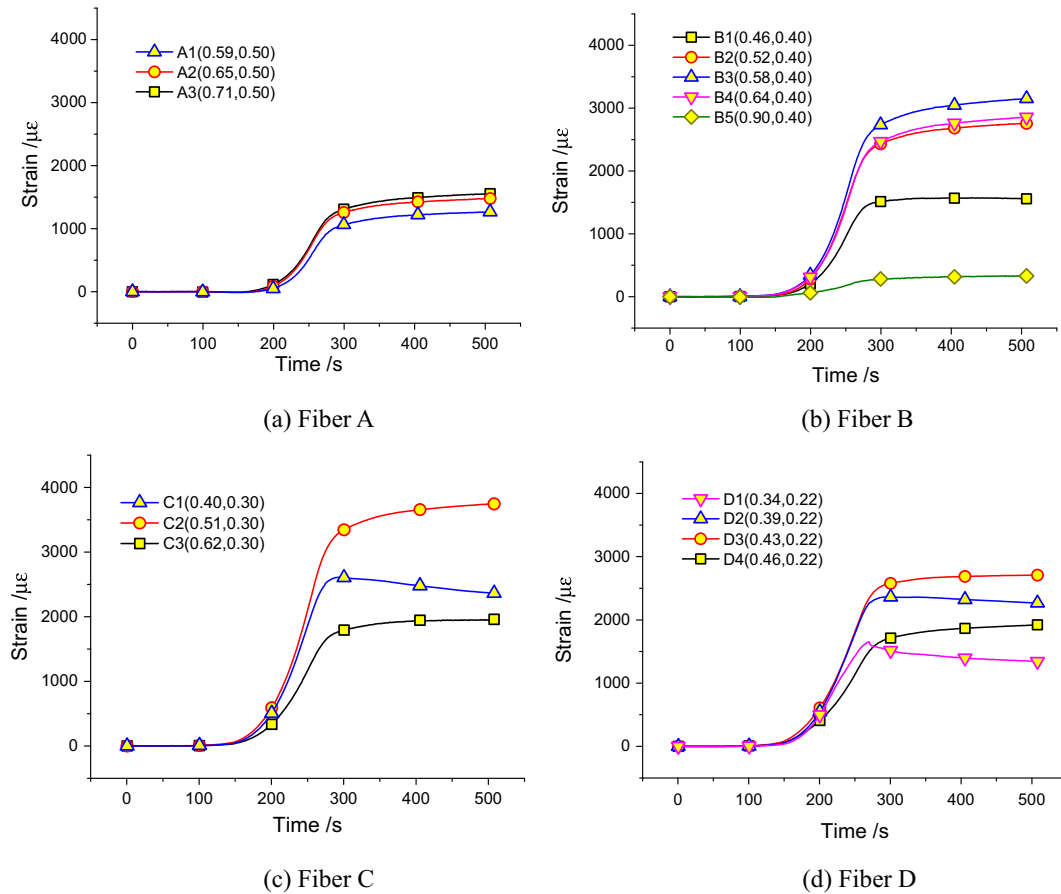
(c) Fiber C

(d) Fiber D

Fig. 9 Strain variations of horizontal FBGs when the g-level was increased from 1 to 10 g. **a** Fiber A. **b** Fiber B. **c** Fiber C. **d** Fiber D

C2 because their strain values were significantly higher than those of other locations. Therefore, the horizontal deformation can be evaluated at a certain height and the potential structural failures in the model can be determined according to the maximum tensile strain value of each sensing fiber.

The changes of the FBG sensors in the vertical fibers differed from those in horizontal fibers. The sensors were in compressive states during the centrifuge test, as shown in Fig. 10, which indicates that the soil was compressed. In general, the compressive strain was small. The largest value was approximately −540 με, which may indicate that the vertical deformation of the soil was relatively small compared with the horizontal deformation. It is also possible that the FBG sensing fibers were not able to measure the compressive deformation accurately because the soil and fiber were too soft and the sensing fibers may have been curved by the soil compression. More investigation on the compressive behavior of the soil and fibers should be conducted to clarify this issue. Similarly, the strain values were different along each single fiber. For Fiber E, the strains of E1 and E2 were larger than that of E3. Similarly, the strain of sensor F1 was higher than those of the other sensors in Fiber F and the strain of sensor G3 was higher than those of the other sensors in Fiber G.

The contours of the strain distribution of the four horizontal cables and three vertical cables are obtained according to the stable strain of the FBGs in one cable at 10 g. The strain values

near the surface and boundary of the slope mode were very small. Prominent tensile strain was located at a distance of approximately 15 cm along the horizontal direction of Fibers B and C, as shown in Fig. 11a, meaning that the horizontal fibers were stretched. It can be concluded that slip deformation appeared at that location. For the vertical fibers, the strain on the surface of the slope was almost zero. Generally, the compressive strain was gradually increasing with the depth of the model because of the high centrifugal force, as shown for Fiber E. However, a distinctly higher compressive strain can be found at a distance of 22 cm along Fiber G, suggesting that the vertical compression of the soil occurred at a potential slip surface, as shown in Fig. 11b. By highlighting the peak strain value of each fiber, the location and the trend of the potential slip surface can be outlined, as shown by the black dashed line in Fig. 11.

Verification

The behavior of the centrifuge slope model was simulated using fast Lagrangian analysis of continua (FLAC) code. Because the mixed soil may have slightly consolidated as a result of the increase of g-level, a strain softening/hardening model was adopted with a Mohr—Coulomb failure criterion. The geometry was the same as that of the centrifuge model and the gravity was increased from 1 to 10 g. A four-node quadrilateral element was used to model the soil. The two vertical sides were assigned a fixed

(a) Fiber E
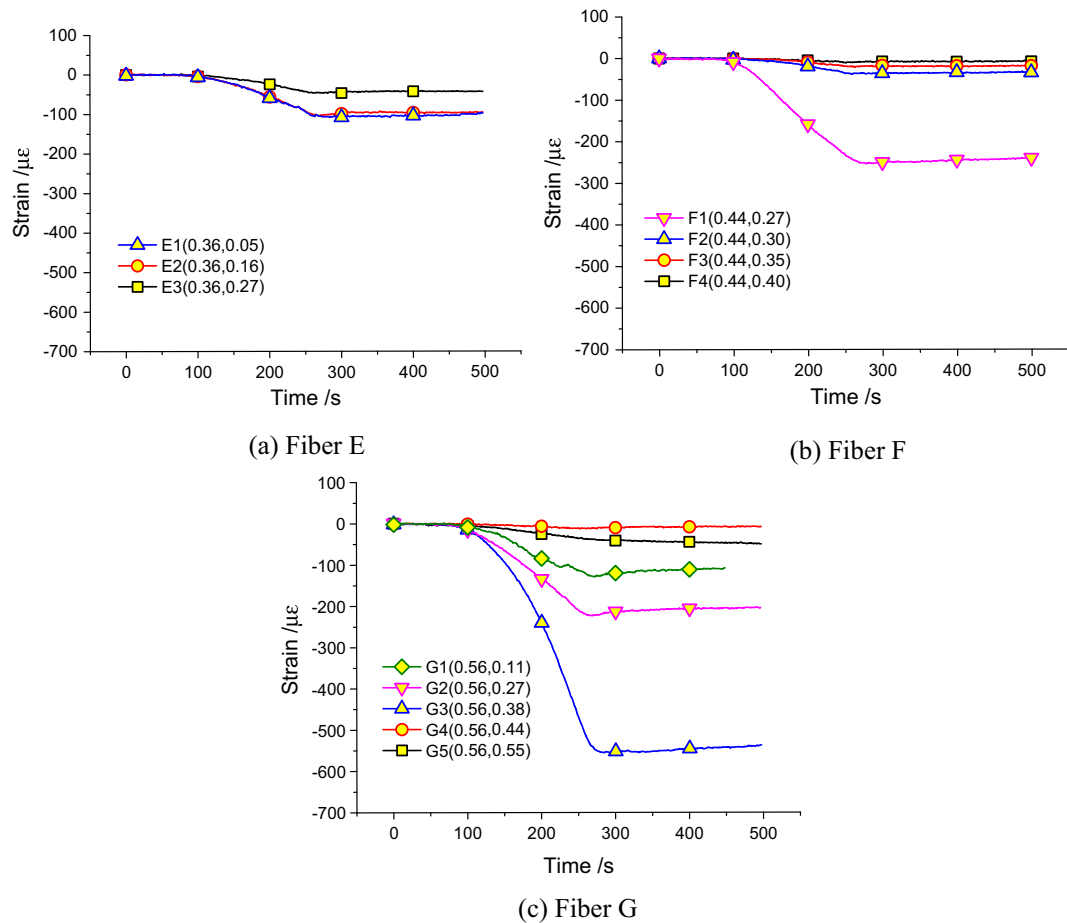
(b) Fiber F

(c) Fiber G

Fig. 10 Strain variations of vertical FBGs when the g-level was increased from 1 to 10 g. **a** Fiber E. **b** Fiber F. **c** Fiber G

displacement boundary condition in the x direction, and the bottom was fixed to prevent movement in both the x and y directions. The slope model had a uniform mesh that was 60 elements wide by 36 elements high. Laboratory tests were conducted on the mixed soil of the centrifuge model to obtain the necessary mechanical parameters, which were adjusted slightly in the numerical simulation for an improved fit to the surface displacements in centrifuge test. The parameters used in the FLAC analysis are listed in Table 2. The comparison between the simulated vertical displacements on the surface of the slope using FLAC and the values measured using the displacement transducers is shown in Fig. 12.

Figure 13a presents the maximum shear strain increment contour when the model was in equilibrium at calculation step of 15,945. The maximum shear strain increment, which is typically derived from displacements, was used to search the potential slip surface. In Fig. 13, the center of the blue circle indicates the positions of FBGs in horizontal fibers, and its diameter shows the strain value when the g-level is 10. By contrast, the FBGs with relatively larger strain values are on or extremely close to the potential slip surface, especially the FBGs on Fibers B and C. The strain values of the FBGs are low when they are far away from the slip surface. However, the maximum strain along Fiber D is not on the simulated potential slip surface. This may be because of the

inhomogeneity of the slope model or because there is more than one potential slip surface in the slope, as a result of which the simulated potential slip surface would not be completely consistent with the actual slip surfaces. Despite this, it is possible to measure the internal strain of the model during the centrifuge test and to predict potential failures, such as slip surfaces, from the strain values of the FBG sensing fibers.

Figure 13b shows a typical comparison between the strain values of FBGs in Fiber B and the horizontal strain distribution of soil along Fiber B, which was calculated according to the horizontal displacement obtained by FLAC. It can be seen that the location of the peak strain is the same. However, the simulated strain at the peak location is larger than that of FBG–B3. The strain values of other FBGs are larger than the simulated values. There are two likely causes. One is a significant difference between the Young's modulus of sensing fibers and that of the soil. The other is slippage between the fiber and soil because the shear strain was very large on the potential slip surface.

Similar results can be found on Fiber C except that the peak of the simulated strain distribution is slightly to the left of the peak of the FBGs. For Fiber A, the peak simulated strain is approximately 3,100 µε, which is larger than the peak strain of the FBGs. For Fiber D, the simulated strain is small because the simulated slip surface is above the sensing Fiber D. However, the peak strain of Fiber D is
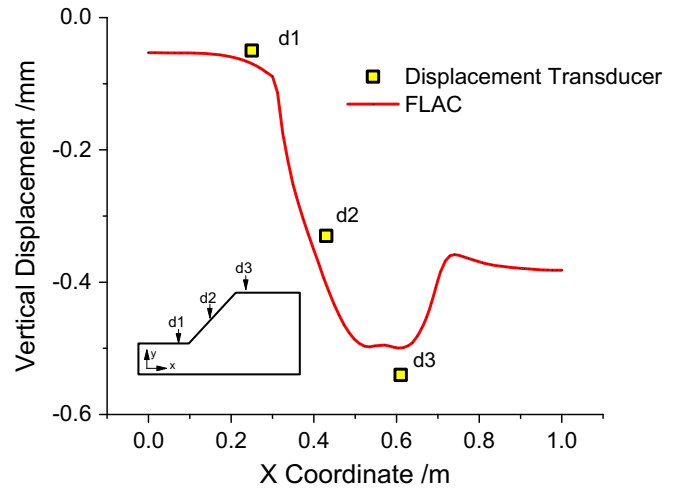
(a) Horizontal strain distribution

(b) Vertical strain distribution
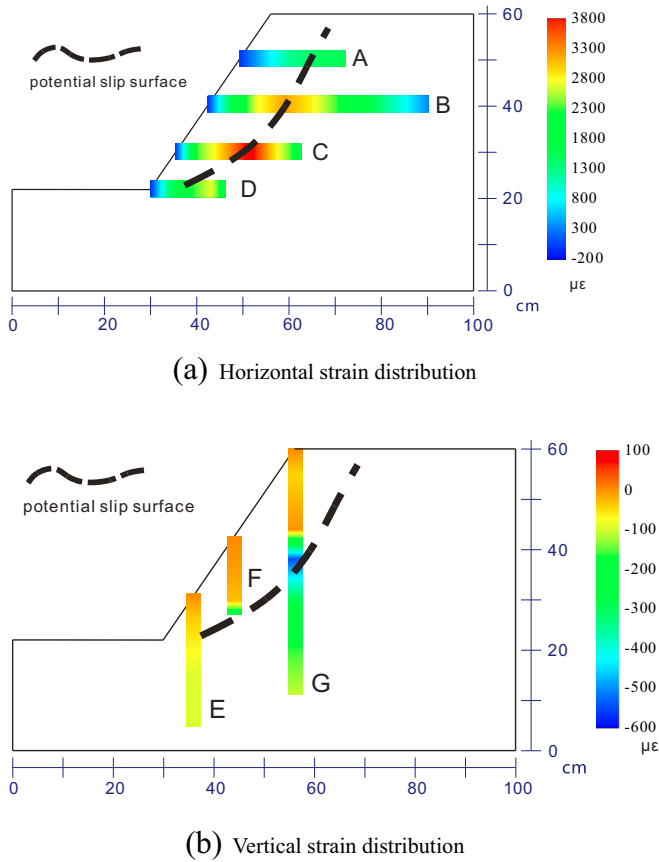
Fig. 11 Strain distribution and potential slip surface when the g-level was 10 g. **a** Horizontal strain distribution. **b** Vertical strain distribution

Fig. 12 Comparison of the simulated vertical displacement on the slope surface using FLAC and the displacements measured using the displacement transducers

2,700 με. As mentioned, this may have been caused the inhomogeneity of the soil or by multiple slip surfaces.

The slope model was compressed in the vertical direction during the centrifuge test. Because Fibers E, F, and G were installed vertically, compressive strain (negative) was expected along the sensing fibers, especially near the slip surface of the slope. However, because the Young's modulus of a sensing fiber is much larger than that of soil, centrifugal force did not compress the sensing fiber when the slope consolidated because of the high g-level. The sensing fiber can be bent on the slip surface if a potential failure can develop; the compressive strain of the sensing fiber may be smaller than that of soil, especially on the slip surface. Figure 13c shows the comparison between the strain measured by FBGs of Fiber G and vertical strain distribution of soil along Fiber G, which is calculated according to the vertical displacement obtained by FLAC. Similar results can also be found for Fibers E and F.

To verify the repeatability of this method of measuring the internal deformation during the flight of a centrifuge model using FBG, the same model was tested again at 10 g after 24 h. A comparison of the FBG strain values of the two tests is shown in

Fig. 14. It can be seen from the data that the strain along the horizontal fibers was tensile and the strain along the vertical fibers was compressive. The location of the peak strain along each sensing fiber was the same as for the first test, namely B3 in Fiber B, C2 in Fiber C, and G3 in Fiber G. Although the strain values of the second test were smaller than those of the first test, especially along the horizontal fibers, the potential slip surface can also be deduced from the peak strains. The fiber strain values can indicate the distribution of the internal deformation in the centrifuge model, as well as the pre-failure deformation values of the potential slip surfaces, which are consistent with those obtained in the first test. The smaller strain values of the second test can be explained by the fact that the soil was consolidated during the first test because compressive strain can be found in the vertical direction, and obvious vertical displacements were observed on the surface of the slope.

There were no visible failures observed during the centrifuge tests at 10 g. Because the interrogator was not specially designed for centrifuge testing, it was dismounted from the centrifuge's central shaft to prevent its destruction during the testing at higher g-levels. Figure 15 shows the cracks on the top of the slope model after an acceleration of 40 g was applied. Obviously, the cracks were the result of shear deformation, which also indicates that more than one slip surface existed in the slope model. One of the cracks was on the potential slip surface that was analyzed above.

When the model was tested at 40 g, the strain of the slope model was large, the strain distribution was highly uneven, and there would produce a nonlinear chirp. Chirped grating has an aperiodic pitch (Grattan and Meggitt 2000), which can be measured by a special interrogator. However, some of the FBG sensors
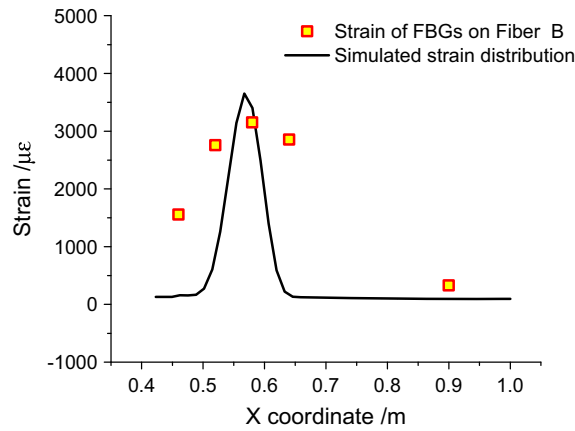
Table 2 Key mechanical parameters of the mixed soil

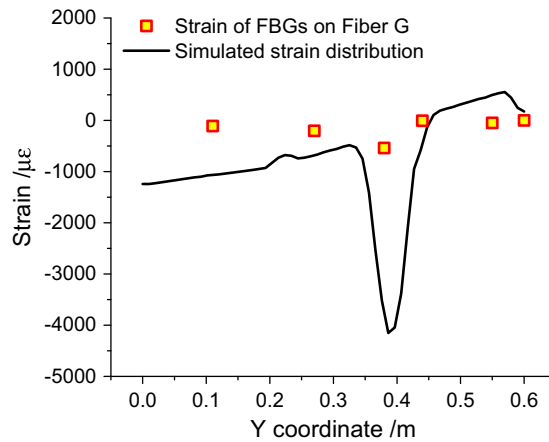| Unit weight γ(kN/m3)	Elastic module E(MPa)	Poisson's ratio	Friction angle Φ(°)	Cohesion c(kPa)
19.6	58.0	0.3	24.0	6.0
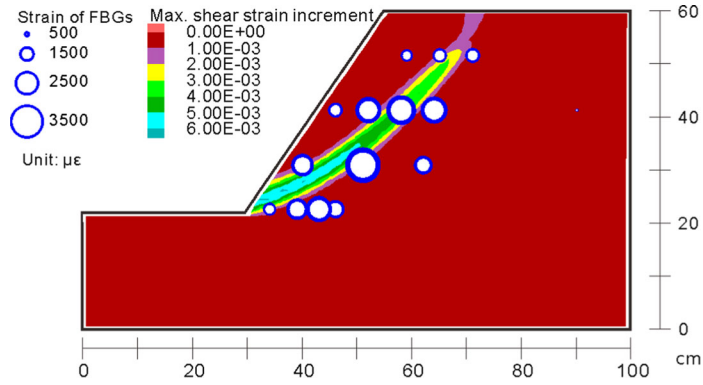
(a) Max shear strain increment and horizontal strain values of the FBG sensors

(b) Strain of FBGs on Fiber B and horizontal strain distribution of soil along Fiber B simulated using
FLAC

(c) Strain of FBGs on Fiber G and vertical strain distribution of soil along Fiber G simulated using
FLAC

Fig. 13 Correspondence between the FBG-measured and FLAC-simulated strain values. **a** Max shear strain increment and horizontal strain values of the FBG sensors. **b** Strain of FBGs on Fiber B and horizontal strain distribution of soil along Fiber B simulated using FLAC. **c** Strain of FBGs on Fiber G and vertical strain distribution of soil along Fiber G simulated using FLAC
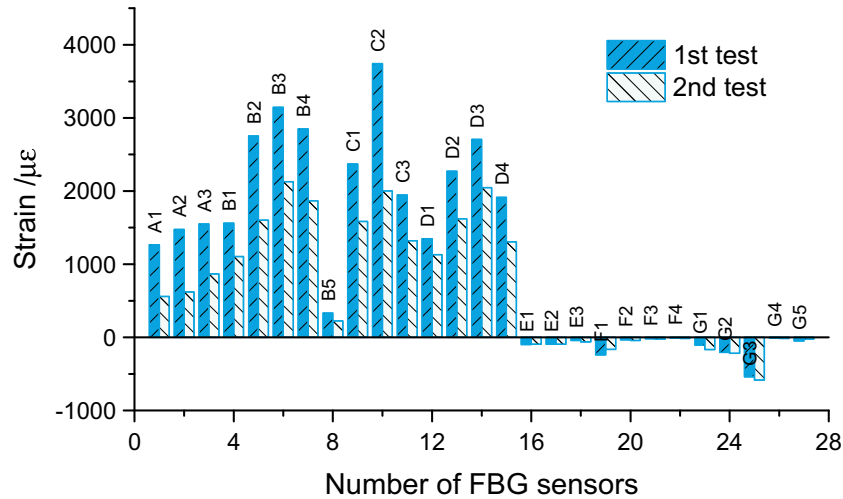
Fig. 14 Comparison of the FBG strains of two tests at 10 g

would be lost because of nonlinear chirp in the test. Therefore, necessary improvements, including enhancements to the interrogator and sensor encapsulation, should be made before the FBG sensing system is used for testing at high g-levels.

Conclusions and discussion

The results of the experiment show that FBG sensing fiber can measure the strain distribution and its variation in a centrifuge model before slippage occurs between the sensing fiber and soil. The comparison with the results of numerical simulation confirms this. A potential failure was predicted from the strain distribution of the fibers. The results of this investigation show that it is feasible to measure the internal deformation of the model during a centrifuge test by using FBG sensing technology. However, it should be noted that optic sensing fibers with FBGs are not suitable for

Fig. 15 Cracks in the top of the slope

applications with large compressive strain values when the fibers are installed in soil directly.

In this preliminary experiment, with an FBG interrogator that was not specifically designed for high centrifugal loads, the maximum g-level was limited to 10 g to avoid destroying the interrogator during the test. Therefore, further investigation should be performed to verify that this system is applicable for high g-level testing. The sensing fibers also should be improved for high g-level testing because some of the FBGs produced chirping after 40 g was applied. Other demodulation technology might be adopted to collect the wavelength changes of the chirped FBGs. Moreover, it should be noted that the sensing fibers may be broken, especially at the gratings. However, FBGs are not necessary to measure high deformations that can be recorded using an extensometer or other sensors on the surface of the model. A contribution of this FBG method is the ability to measure extremely small deformations inside the model during centrifuge testing. The size effects of the sensing fibers can be neglected. If it were possible, it might be preferable to design different types of sensing fibers suitable for the deformation behavior of the centrifuge model.

In addition, FBG sensing technology can be attached to geotechnical structures, such as piles, anchors, tunnels, and retaining walls, to measure the strain, pressure, and deformation values of those structures. This application of FBG technology represents a new method to analyze the behavior of a centrifuge model.
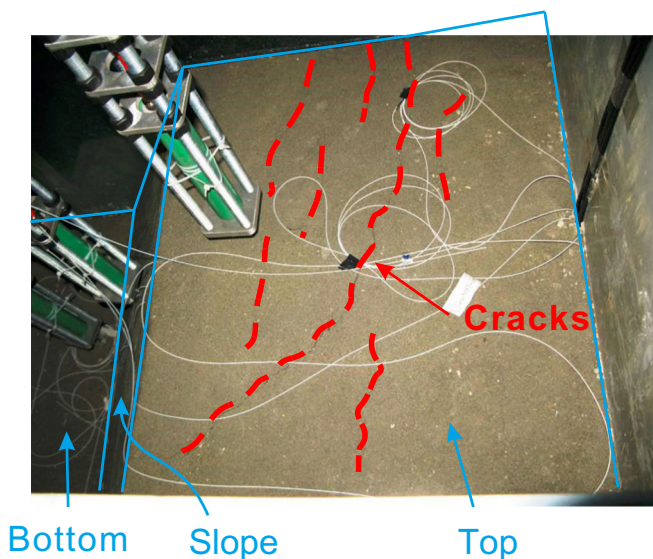
for the sensing fibers with FBGs and to MOI Beijing Representative Office for the FBG interrogator.

References

Ansari F (2007) Practical implementation of optical fiber sensors in civil structural health monitoring. J Intell Mater Syst Struct 18(8):879–889

Arsenault TJ, Achuthan A, Marzoccal P, Grappasonni, Coppotelli G (2013) Development of a FBG based distributed strain sensor system for wind turbine structural health monitoring. Smart Mater Struct 22:075027

Bao XY, Chen L (2012) Recent progress in distributed fiber optic sensors. Sensors 12:8601–8639

Elshafie MZEB, Choy CKC, Mair RJ (2013) Centrifuge modeling of deep excavations and their interaction with adjacent buildings. Geotech Test J 36(5):1–12

Grattan KTV, Meggitt BT (2000) Optical fiber sensor technology: advanced applications — Bragg gratings and distributed sensors. Springer, US

Habel WR, Hofmann D, Döring H, Jentsch H, Senze A, Kowalle G (2014) Detection of a slipping soil area in an open coal pit by embedded fibre-optic sensing rods. Proceeding of the 5th International forum on opto-electronic sensor-based monitoring in geo-engineering, Nanjing, China, 1–7

Hauswirth D, Iten M, Richli R, Puzrin AM (2010) Fibre optic cable and micro-anchor pullout tests in sand. Proceedings of the 7th International Conference on Physical Modelling in Geotechnics (ICPMG 2010), Zurich, Switzerland

Hill KO, Fujii Y, Johnson DC, Kawasaki BS (1978) Photosensitivity in optical fiber waveguides: application to reflection filter fabrication. Appl Phys Lett 32:647–649

Hill KO, Malo B, Bilodeau F, Johnson DC, Albert J (1993) Bragg gratings fabricated in monomode photosensitive optical fiber by UV exposure through a phase mask. Appl Phys Lett 62(10):1035–1037

Kruse GAM, Bezuijen A (1998) The use of CT scans to evaluate soil models. Proc. Of Centrifuge 98, Balkema, pp 79–84

Ling HI, Wu MH, Leshchinsky D, Leshchinsky B (2009) Centrifuge modeling of slope instability. J Geotech Geoenviron Eng 135:758–767

Lu Y, Shi B, Wei GQ, Chen SE, Zhang D (2012) Application of a distributed optical fiber sensing technique in monitoring the stress of precast piles. Smart Mater Struct 21:115011

Muir Wood D (2004) Geotechnical modelling. Spon Press, London and New York

Ng CWW, Shi JW, Hong Y (2013a) Three-dimensional centrifuge modelling of basement excavation effects on an existing tunnel in dry sand. Can Geotech J 50:874–888

Ng CWW, Boonyarak T, Mašín D (2013b) Three-dimensional centrifuge and numerical modeling of the interaction between perpendicularly crossing tunnels. Can Geotech J 50:935–946

Niewczas P, McDonald JR (2007) Advanced optical sensors for power and energy systems applications. IEEE Instrumentation & Measurement Magazine (1):18–28

Ortigao JAR, Sayao ASFJ (2004) Handbook of slope stabilisation. Springer- Verlag Berlin Heidelberg, New York

Rao YJ, Lobo Ribeiro AB, Jackson DA, Zhang L, Bennion I (1995) Combined spatial- and time-division-multiplexing scheme for fibre grating sensors with drift-compensated phase-sensitive detection. Opt Lett 20:2149

Sun YJ, Zhang D, Shi B, Tong HJ, Wei GQ, Wang X (2014) Distributed acquisition, characterization and process analysis of multi-field information in slopes. Eng Geol 182:49–62

Shi B, Zhang D, Zhu HH, Liu C (2011) Application of distributed optical fiber strain measurement into geotechnical engineering monitoring. In: Chang FK (ed) Proceedings of the 8th international workshop on structural health monitoring, vol 2. Stanford University, USA, p. 2327

Sommers AN, Viswanadham BVS (2009) Centrifuge model tests on the behavior of strip footing on geotextile-reinforced slopes. Geotext Geomembr 27:497–505

Take WA, Bolton MD, Wong PCP, Yeung FJ (2004) Evaluation of landslide triggering mechanisms in model fill slopes. Landslides 1(3):173–184

Wang BJ, Li K, Shi B, Wei GQ (2009) Test on application of distributed fiber optic sensing technique into soil slope monitoring. Landslides 6(1):61–68

White DJ, Bolton MD (2002) Soil deformation around a displacement pile in sand. Physical modelling in geotechnics: ICPMG'02, Newfoundland, pp 649–654

Yin YP, Wang HD, Gao YL, Li X (2010) Real-time monitoring and early warning of landslides at relocated Wushan town, the three gorges reservoir, China. Landslides 7(3):339–349

Zornberg JG, Mitchell JK, Sitar N (1997) Testing of reinforced slopes in a geotechnical centrifuge, geotechnical testing journal. ASTM 20(4):470–480

D. Zhang (✉) · **H. Wang**
School of Earth Sciences and Engineering,
Nanjing University,
Nanjing, 210023, China
e-mail: zhangdan@nju.edu.cn

Q. Xu · **G. Zheng**
State Key Laboratory of Geohazard Prevention and Geoenvironment Protection (SKLGP),
Chengdu University of Technology,
Changdu, 610059, China

A. Bezuijen
Department of Civil Engineering,
Ghent University,
B-9052, Gent, Belgium